Letter

Effect of cluster transfer on the production of neutron-rich nuclides near $N = 126$ in multinucleon-transfer reactions

Zhao-Qing Feng [*]
School of Physics and Optoelectronics, South China University of Technology, Guangzhou 510640, China

(Received 8 July 2023; revised 19 September 2023; accepted 17 October 2023; published 13 November 2023)

The cluster transfer in multinucleon-transfer reactions near Coulomb barrier energies is implemented into the master equations in the dinuclear system model, in which deuterons, tritons, ^{3}He, and α particles are taken into account. The effects of cluster transfer and dynamical deformation on the formation of primary and secondary fragments are systematically investigated. It is found that the inclusion of cluster transfer is favorable for fragment formation by increasing the transferring nucleons and leads to a broad mass distribution. The isotopic cross sections of wolfram, osmium, radon, and francium in ^{136}Xe + ^{208}Pb reactions at an incident energy of $E_{\mathrm{c.m.}} = 450$ MeV are nicely consistent with the Argonne data. The new neutron-rich isotopes of wolfram and osmium are predicted with cross sections above 10 nb. The production mechanism of neutron-rich heavy nuclei near $N = 126$ in ^{58,64,72}Ni + ^{198}Pt reactions is investigated thoroughly. The cross sections for producing the neutron-rich isotopes of platinum, iridium, osmium, and rhenium in the multinucleon-transfer reactions ^{64}Ni + ^{198}Pt and ^{72}Ni + ^{198}Pt at center-of-mass energies of 220 and 230 MeV are estimated and proposed for future experiments.

DOI: 10.1103/PhysRevC.108.L051601

The completeness of the periodic table of elements and the origin of heavy elements in the universe are basic science problems [1], which are associated with the synthesis of superheavy elements, the rapid-neutron capture process in the big-bang nucleosynthesis, shell evolution, nuclear fission, etc. In terrestrial laboratories, neutron-rich heavy or superheavy nuclei might be created via different ways, i.e., the projectile fragmentation reactions, spallation and fission reactions of heavy nuclei, the fusion-evaporation reaction, the multinucleon-transfer reaction, etc. The fusion-evaporation reactions, namely, the cold fusion reactions with ^{208}Pb- or ^{209}Bi-based targets [2–5] and the ^{48}Ca-induced warm reactions [6–8], have been extensively used for synthesizing superheavy nuclei (SHN). The heavy nuclides created by the fusion-evaporation reactions are located in the neutron-deficient regime in the nuclear chart and away from the "island of stability" [9,10]. Up to now, roughly 3200 nuclides have been created in different laboratories in the world via projectile fragmentation, spallation and fission reactions of heavy nuclei, the fusion-evaporation reaction, the transfer reaction, etc. [11]. Recently, the multinucleon-transfer (MNT) reaction has attracted much attention for producing neutron-rich heavy and superheavy nuclei. With the construction of new facilities in the world such as RIBF (RIKEN, Japan) [12], SPIRAL2 (GANIL in Caen, France) [13], FRIB (MSU, USA) [14], and HIAF (IMP, China) [15], SHN on the island of stability might be synthesized in experiments by using neutron-rich radioactive-beam-induced fusion reactions or via MNT reactions. The spectroscopic measurements of neutron-rich heavy nuclei near $N = 126$, 152, and 162 are particular important for understanding single-particle motion, shape coexistence, the new decay mode beyond the binary fission, etc.

Since the 1970s, MNT reactions or deep inelastic heavy-ion collisions have been extensively investigated in experiments, in which new neutron-rich isotopes of light nuclei and also proton-rich actinide nuclei have been observed [16–22]. Recently, MNT reactions have attracted attention again in experiments for the production of new neutron-rich isotopes. It has been found that MNT reactions have the advantage of broad isotope distribution, e.g., more than 100 nuclides with $Z = 82$–100 in the ^{48}Ca + ^{248}Cm reaction [23]. The production cross sections, total kinetic energy spectra, and angular distributions were measured in the following reactions: ^{136}Xe + ^{208}Pb [24,25], ^{136}Xe + ^{198}Pt [26,27], ^{156,160}Gd + ^{186}W [28], and ^{238}U + ^{232}Th [29]. Recently, the new isotope ^{241}U was created in MNT reactions of ^{238}U + ^{198}Pt with the KEK Isotope Separation System installed at RIKEN [30]. The neutron-rich nuclides near the neutron shell closure with $N = 126$ have significant application in understanding the origin of heavy elements from iron to uranium in the r-process of nucleosynthesis in stellar evolution. It has been confirmed that shell closure plays an important role in the production of neutron-rich nuclei and has more advantage with the MNT reactions in comparison to projectile fragmentation [31]. MNT reactions with neutron-rich radioactive beams have more advantages for creating rare isotopes beyond the β-stability line. Several models have been proposed for describing the MNT reactions, i.e., the dinuclear system (DNS) model [32–34], the GRAZING model [35,36], the dynamical model based on multidimensional Langevin equations [37–39], etc. Moreover, the microscopic approaches

[*]Corresponding author: fengzhq@scut.edu.cn

based on the nucleon degree of freedom, the time-dependent Hartree-Fock approach [40–43] and its extension by incorporating fluctuation and correlation in the nuclear transfer based on the stochastic mean-field theory [44], and improved quantum molecular dynamics [45–47] are also used to describe MNT reactions. Some interesting issues have been investigated with the models, e.g., the production cross sections of new isotopes, kinetic energy spectra and polar angle distribution of MNT fragments, the structure effect on the fragment formation, preequilibrium cluster emission, etc.

In this Letter, the cluster transfer in solving the master equations has been implemented into the DNS model for the first time, in particular, for transferring deuterons, tritons, ^{3}He, and α particles. MNT dynamics is investigated with the DNS-cluster model. In the DNS model, nucleon transfer between the binary fragments is governed by a single-particle Hamiltonian [48]. Only nucleons within the valence space are active for transfer [49,50]. The transition probability is related to the local excitation energy and nucleon transfer [48,51], which is microscopically derived from the interaction potential in valence space. The local excitation energy is determined by the dissipation energy from the relative motion and the potential energy surface of the DNS. The dissipation of the relative motion and angular momentum of the DNS is described by the classical trajectory approach. The cross sections of the primary fragments (Z_1, N_1) are calculated as follows:

$$\sigma_{\mathrm{pr}}(Z_1, N_1, E_{\mathrm{c.m.}}) = \sum_{J=0}^{J_{\max}} \sigma_{\mathrm{cap}}(E_{\mathrm{c.m.}}, J) \int f(B) \times P(Z_1, N_1, E_1, J_1, B) dB. \quad (1)$$

The secondary decay of the primary fragments is considered to form the final MNT fragments. The cross section is evaluated by

$$\sigma_{\mathrm{sur}}(Z_1, N_1, E_{\mathrm{c.m.}}) = \sum_{J=0}^{J_{\max}} \sigma_{\mathrm{cap}}(E_{\mathrm{c.m.}}, J) \int f(B) \times \sum_s P(Z_1', N_1', E_1', J_1', B) \times W_{\mathrm{sur}}(Z_1', N_1', E_1', J_1', s) dB. \quad (2)$$

Here, E_1 and J_1 respectively denote the excitation energy and the angular momentum for the fragments (Z_1, N_1), which are related to the center-of-mass energy $E_{\mathrm{c.m.}}$ and the incident angular momentum J. The evaporation channel s (Z_s, N_s) might be γ particles, neutrons, charged particles, etc., emitted from the excited MNT fragments with the relations $Z_1 = Z_1' - Z_s$ and $N_1 = N_1' - N_s$. The maximal angular momentum $J_{\max}$ is taken to be the grazing collision of two colliding nuclei. The capture cross section is given by $\sigma_{\mathrm{cap}} = \pi\hbar^2(2J+1)T(E_{\mathrm{c.m.}}, J)/(2\mu E_{\mathrm{c.m.}})$ and the probability $T(E_{\mathrm{c.m.}}, J)$ is calculated within the Hill-Wheeler formula. For the heavy system, there is no potential pocket after overcoming the Coulomb barrier, e.g., the systems ^{136}Xe + ^{208}Pb, ^{238}U + ^{198}Pt, etc. The classical trajectory approach is used with the relations $T(E_{\mathrm{c.m.}}, J) = 0$ and $T(E_{\mathrm{c.m.}}, J) = 1$ for $E_{\mathrm{c.m.}} < B + J(J+1)\hbar^2/(2\mu R_C^2)$ and $E_{\mathrm{c.m.}} > B + J(J+1)\hbar^2/(2\mu R_C^2)$, respectively. The μ and R_C denote the reduced mass and the Coulomb radius by $\mu = m_n A_p A_t/(A_p + A_t)$, with m_n, A_p, and A_t being the nucleon mass and the numbers of projectile and target nuclides, respectively. The distribution function is taken as the Gaussian form $f(B) = \frac{1}{N}\exp\{-[(B - B_m)/\Delta]^2\}$, with the normalization constant satisfying the unity relation $\int f(B)dB = 1$. The quantities B_m and Δ are evaluated by $B_m = (B_C + B_S)/2$ and $\Delta = (B_C - B_S)/2$, respectively. B_C and B_S are the Coulomb barrier in the waist-to-waist collisions and the minimum barrier obtained by varying the quadrupole deformation of the colliding partners [51].

The distribution probability is obtained by solving a set of master equations numerically in the potential energy surface of the DNS. The temporal evolution of the distribution probability $P(Z_1, N_1, E_1, \beta_1, B, t)$ for fragment 1 with the proton number Z_1, the neutron number N_1, the excitation energy E_1, and the quadrupole deformation β_1 is described by the following master equation:

$$\begin{aligned}
\frac{dP(Z_1, N_1, E_1, \beta_1, B, t)}{dt} = & \sum_{Z_1'=Z_1\pm1} W_{Z_1,N_1,\beta_1;Z_1',N_1,\beta_1'}(t)[d_{Z_1,N_1}P(Z_1', N_1, E_1', \beta_1', B, t) - d_{Z_1',N_1}P(Z_1, N_1, E_1, \beta_1, B, t)] \\
& + \sum_{N_1'=N_1\pm1} W_{Z_1,N_1,\beta_1;Z_1,N_1',\beta_1'}(t)[d_{Z_1,N_1}P(Z_1, N_1', E_1', \beta_1', B, t) - d_{Z_1,N_1'}P(Z_1, N_1, E_1, \beta_1, B, t)] \\
& + \sum_{Z_1'=\pm1, N_1'=N_1\pm1} W^d_{Z_1,N_1,\beta_1;Z_1',N_1',\beta_1'}(t)[d_{Z_1,N_1}P(Z_1', N_1', E_1', \beta_1', B, t) - d_{Z_1',N_1'}P(Z_1, N_1, E_1, \beta_1, B, t)] \\
& + \sum_{Z_1'=\pm1, N_1'=N_1\pm2} W^t_{Z_1,N_1,\beta_1;Z_1',N_1',\beta_1'}(t)[d_{Z_1,N_1}P(Z_1', N_1', E_1', \beta_1', B, t) - d_{Z_1',N_1'}P(Z_1, N_1, E_1, \beta_1, B, t)] \\
& + \sum_{Z_1'=\pm2, N_1'=N_1\pm1} W^{^3He}_{Z_1,N_1,\beta_1;Z_1',N_1',\beta_1'}(t)[d_{Z_1,N_1}P(Z_1', N_1', E_1', \beta_1', B, t) - d_{Z_1',N_1'}P(Z_1, N_1, E_1, \beta_1, B, t)] \\
& + \sum_{Z_1'=\pm2, N_1'=N_1\pm2} W^\alpha_{Z_1,N_1,\beta_1;Z_1',N_1',\beta_1'}(t)[d_{Z_1,N_1}P(Z_1', N_1', E_1', \beta_1', B, t) - d_{Z_1',N_1'}P(Z_1, N_1, E_1, \beta_1, B, t)].
\end{aligned} \quad (3)$$

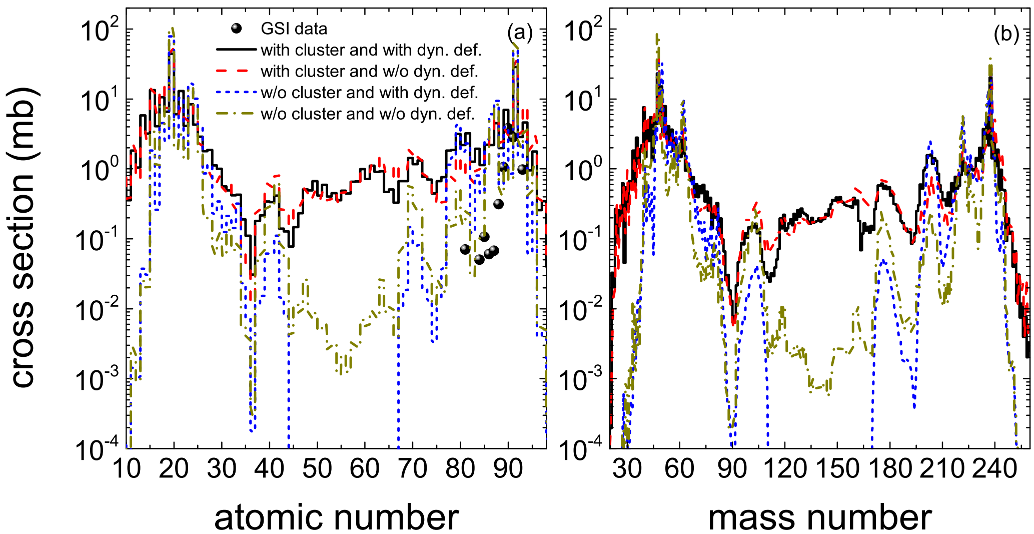

FIG. 1. Comparison of the MNT fragments in collisions of $^{48}Ca + ^{238}U$ at the beam energy of 4.76 MeV/nucleon with different cases of cluster transfer (deuteron, triton, ^{3}He, and α particle) and dynamical evolution of quadrupole deformation of DNS fragments. The available experimental data are taken from Ref. [55].

Here $W_{Z_1,N_1,\beta_1;Z_1',N_1,\beta_1'}$ ($W_{Z_1,N_1,\beta_1;Z_1,N_1',\beta_1'}$) is the mean transition probability from the channel (Z_1, N_1) with the energy E_1 and the quadrupole deformation β_1 to the DNS fragment (Z_1', N_1) with E_1' and β_1' by transferring a proton [or (Z_1, N_1) to (Z_1, N_1') by transferring a neutron]. The cluster transition probabilities by transferring deuterons, tritons, ^{3}He, and α particles are denoted by $W^d_{Z_1,N_1,\beta_1;Z_1',N_1',\beta_1'}(t)$, $W^t_{Z_1,N_1,\beta_1;Z_1',N_1',\beta_1'}(t)$, $W^{^3He}_{Z_1,N_1,\beta_1;Z_1',N_1',\beta_1'}(t)$, and $W^{\alpha}_{Z_1,N_1,\beta_1;Z_1',N_1',\beta_1'}(t)$ from channel (Z_1, N_1) to channel (Z_1', N_1'), respectively.

The microscopic dimension d_{Z_1,N_1} corresponds to the DNS fragment (Z_1, N_1, E_1, β_1). The nucleon or cluster transfer is considered by the relations $Z_1' = Z_1 \pm Z_\nu$ and $N_1' = N_1 \pm N_\nu$ with the proton number Z_ν and the neutron number N_ν, in which the nucleon transfer by neutrons, protons, deuterons, tritons, ^{3}He, and α particles are taken into account in the process of solving the master equations. At the initial time, the distribution probabilities of projectile and target nuclei are set to be $P(Z_{\rm proj}, N_{\rm proj}, E_1 = 0, \beta_1 = \beta_{\rm proj}, B, t = 0) = 0.5$ and $P(Z_{\rm targ}, N_{\rm targ}, E_1 = 0, \beta_1 = \beta_{\rm targ}, B, t = 0) = 0.5$. The unitary condition is also satisfied by the relation $\sum_{Z_1,N_1} P(Z_1, N_1, E_1, \beta_1, B, t) = 1$ during the time evolution in the relaxation process after the inclusion of cluster transfer.

Similar to the sequential nucleon transfer [51], the cluster-transfer dynamics in the interacting binary fragments is described by a single-particle Hamiltonian. The transition probabilities of neutrons, protons, deuterons, tritons, ^{3}He, and α particles are related to the local excitation energy, which is microscopically estimated from the interaction potential in valence space as

$$W^{\nu}_{Z_1,N_1;Z_1',N_1'} = G_\nu \frac{\tau_{\rm mem}(Z_1, N_1, E_1; Z_1', N_1', E_1')}{d_{Z_1,N_1} d_{Z_1',N_1'} \hbar^2} \sum_{ii'} |\langle i'|V|i\rangle|^2, \tag{4}$$

with $Z_1' = Z_1 \pm Z_\nu$ and $N_1' = N_1 \pm N_\nu$. Z_ν and N_ν are the proton and neutron numbers for transferring a cluster, respectively. The spin-isospin statistical factors G_ν are taken to be 1, 1, 3/8, 1/12, 1/12, and 1/96, corresponding to protons, neutrons, deuterons, tritons, ^{3}He, and α particles, respectively, which rely on the Wigner density approach for recognizing the clusters in heavy-ion collisions [52,53]. It should be noticed that the transition probability rapidly decreases with the mass number of the transferring cluster.

The memory time is related to the interaction potential and estimated by [54]

$$\tau_{\rm mem}(Z_1, N_1, E_1; Z_1', N_1', E_1') = \left[\frac{2\pi\hbar^2}{\sum_{KK'}\langle V_{KK} V^*_{KK'}\rangle}\right]^{1/2}, \tag{5}$$

$$\langle V_{KK} V^*_{KK'}\rangle = \tfrac{1}{4} U^2_{KK'} g_K g_{K'} \Delta_{KK'} \Delta\varepsilon_K \Delta\varepsilon_{K'} \times \left[\Delta^2_{KK'} + \tfrac{1}{6}[(\Delta\varepsilon_K)^2 + (\Delta\varepsilon_{K'})^2]\right]^{-1/2}. \tag{6}$$

The interaction matrix element in Eq. (4) is given by

$$\sum_{ii'} |\langle i'|V|i\rangle|^2 = \omega_{11}(ii) + \omega_{22}(i'i') + \omega_{12}(ii') + \omega_{21}(i'i), \tag{7}$$

in which the element is calculated by

$$\omega_{KK'}(i, i') = d_{Z_1,N_1} \langle V_{KK'} V^*_{KK'}\rangle \tag{8}$$

with the states $i(Z_1, N_1, E_1)$ and $i'(Z_1', N_1', E_1')$. In the relaxation process of the relative motion, the DNS will be excited by the dissipation of the relative kinetic energy. The local excitation energy is determined by the dissipation energy from the relative motion and the potential energy surface of the DNS [48].

The MNT reactions have been extensively investigated both in experiments and in theories. The reaction mechanism has been considered a unique way to reach the neutron-rich heavy nuclei, even the "island of stability" of superheavy nuclides in the nuclear chart, i.e., near the neutron shell closure with $N = 126$, 152, and 162. To describe the MNT reactions in theories, sophisticated transport models are still

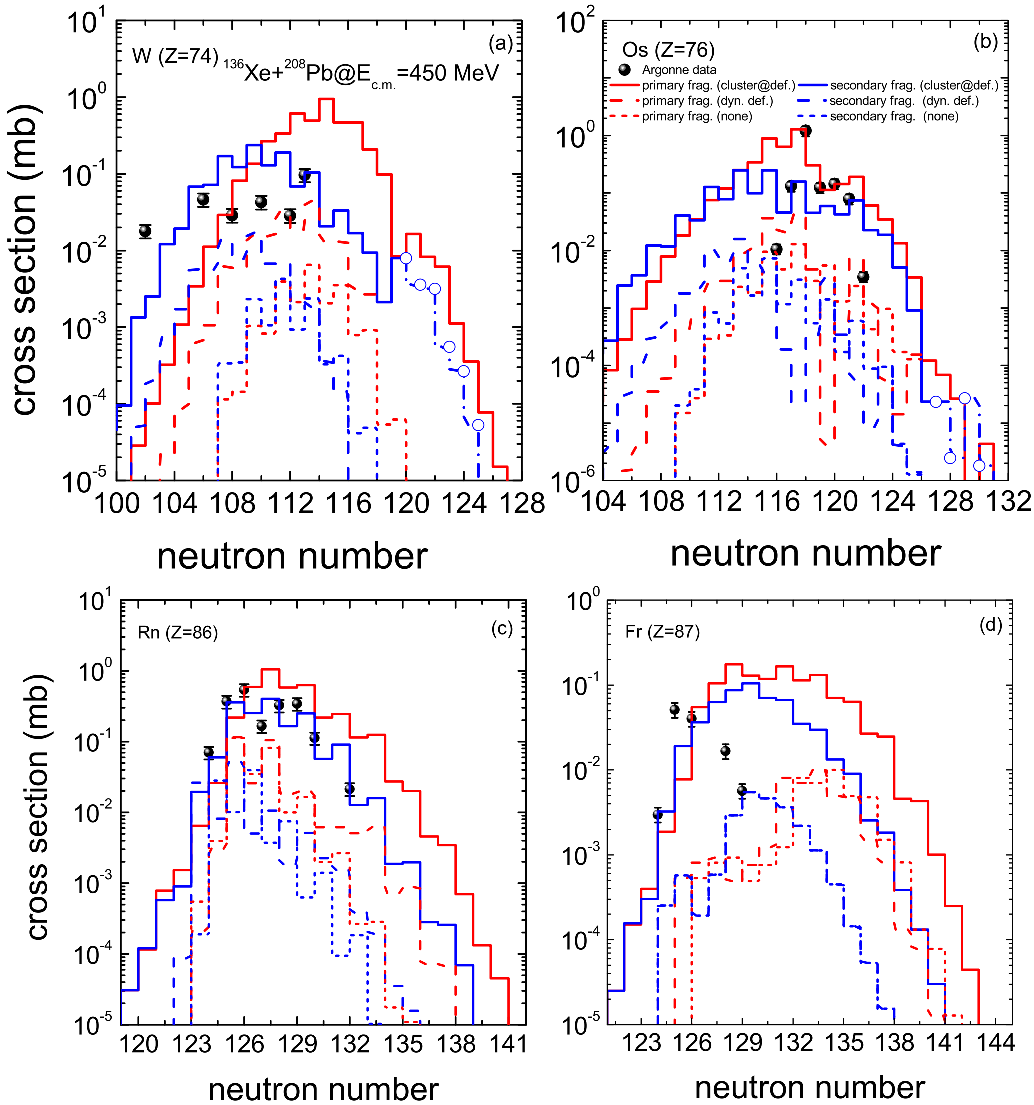

FIG. 2. Isotopic distributions of the primary and secondary fragments for (a) wolfram (W), (b) osmium (Os), (c) radon (Rn), and (d) francium (Fr) production in the MNT reactions of ^{136}Xe + ^{208}Pb at $E_{c.m.}$ = 450 MeV with the effects of cluster transfer and dynamical deformation and compared with the Argonne data [25]. The open symbols denote the new isotopes [59].

expected for describing the collision dynamics. The dinuclear system model has been extensively used for estimating the SHN production cross section in cold-fusion reactions with ^{208}Pb and ^{209}Bi targets, in ^{48}Ca-induced fusion reactions, and for modeling the MNT reaction dynamics. As a test of the DNS model, the available data at GSI in collisions of ^{48}U + ^{248}Cm at the beam energy of $E_{\mathrm{lab}} = 4.76$ MeV/nucleon ($E_{\mathrm{c.m.}} = 190.1$ MeV, $V_{\text{tip-tip}} = 172.1$ MeV, and $V_{\text{waist-waist}} = 184.6$ MeV) are compared with the calculations as shown in Fig. 1. It should be noticed that the products of MNT fragments were populated by the differential cross sections at the SHIP acceptance angle of $0^\circ \pm 2^\circ$ towards the beam direction [55]. The effects of cluster transfer and dynamical quadrupole deformation are coupled to the dissipation of the relative motion energy and the angular momentum. The bump structure of the charged numbers of MNT fragments is caused from the shell effects, i.e., with the numbers $Z = 28$, 50, and 82, which is favorable for the fragment formation because of the larger distribution probability and survival against the particle evaporation. Overall, the broader charge and mass distributions are obtained with the cluster transfer taken into account in the DNS model. It should be noticed that the consideration of sole nucleon transfer and dynamical deformation enable the nearly symmetric distributions of the charge and mass spectra. The cluster transfer is more pronounced in the targetlike region (heavier fragments) and leads to the broader mass distribution. The overestimation of the production cross sections in the targetlike region in comparison with the GSI data is caused from the forward measurements of MNT fragments. It is well known that the MNT fragments manifest the anisotropic distribution, and the angular distributions of the projectilelike and targetlike fragments are related to the beam energy [24,56,57].

The neutron closed shell $N = 126$ is particularly significant for stabilizing and elongating the lifetime of neutron-rich isotopes via the MNT reactions, which play an essential role

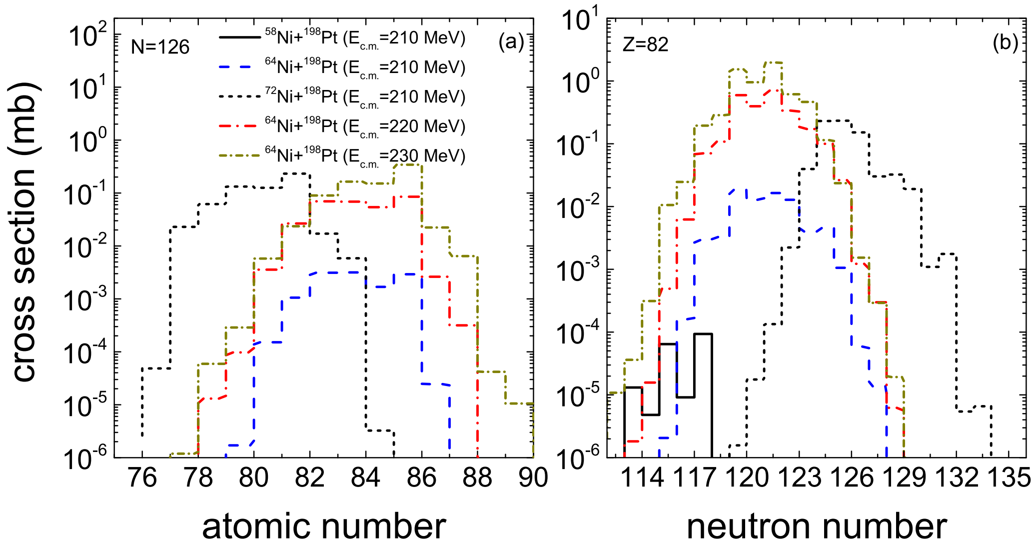

FIG. 3. The secondary fragment production in the MNT reactions of $^{58,64,72}Ni + ^{198}Pt$ near the shell closure with $N = 126$ (s) and $Z = 82$ (b), respectively.

for the production of heavy elements beyond the iron element in stellar nucleosynthesis through the *r*-process at the "waiting point." The low-energy MNT reaction of $^{136}Xe + ^{208}Pb$ for production of new heavy isotopes was proposed by Zagrebaev and Greiner for the first time with the multidimensional Langevin approach [58]. The isotopic and isotonic distributions of MNT products are of importance to investigate the shell evolution with varying the neutron and proton numbers of fragments, nuclear spectroscopies via the decay modes, reaction dynamics associated with the neck evolution, nucleon or cluster transfer, and temporal evolutions of deformation parameters (quadrupole, octupole, and hexadecapole). The influence of cluster transfer and dynamical deformation on the MNT fragment formation in the reaction of $^{136}Xe + ^{208}Pb$ is investigated. Shown in Fig. 2 is the isotopic distributions of the primary (red lines) and secondary (blue lines) fragments for wolfram (W), osmium (Os), radon (Rn), and francium (Fr) production in the MNT reactions of

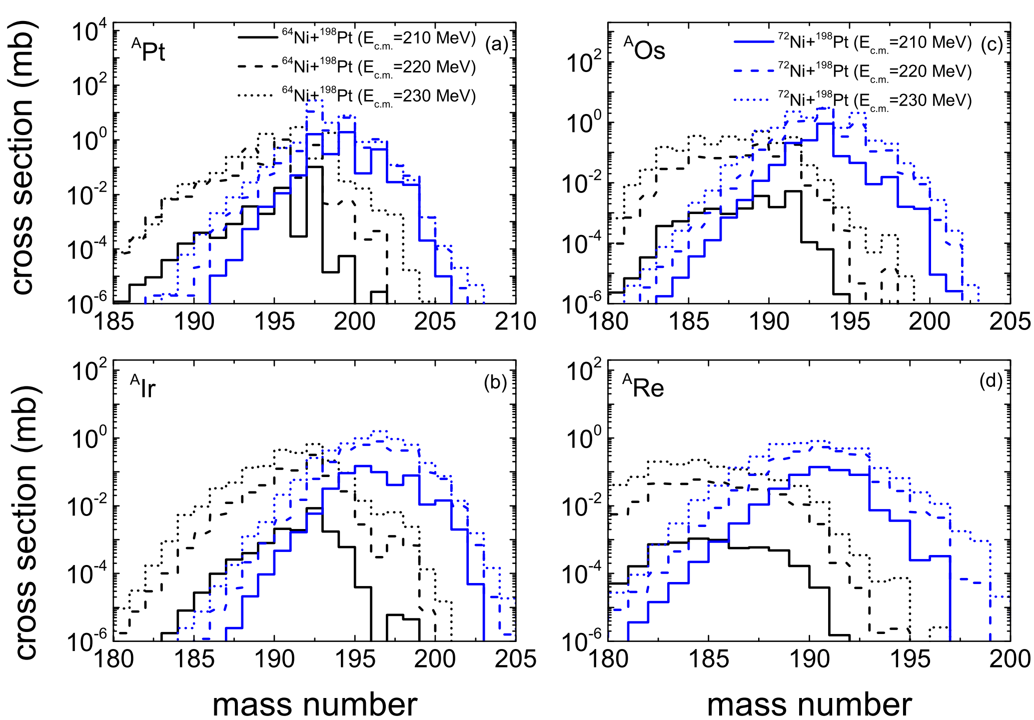

FIG. 4. Isotopic distributions of platinum (Pt), iridium (Ir), osmium (Os), and rhenium (Re) in the MNT reactions of $^{64}Ni + ^{198}Pt$ and $^{72}Ni + ^{198}Pt$ at center-of-mass energies of 210, 220, and 230 MeV, respectively.

$^{136}Xe + ^{208}Pb$ at $E_{c.m.} = 450$ MeV above the touching barrier ($V_T = 427.3$ MeV). It is obvious that the primary fragments manifest the larger cross sections of the neutron-rich isotope production, e.g., the maximal positions around the isotopes ^{188}W and ^{194}Os for the eight- and six-proton pickup reactions. The secondary decay by evaporating several neutrons enables maximal yields close to the β-stability line. The inclusion of the cluster transfer and dynamical deformation leads to the broader isotope distribution with cross sections above 10 nb and is more consistent with the Argonne data [25]. The new isotopes might be created via the MNT reactions with possible measurements in experiments [59], i.e., from 8 μb for ^{194}W to 4.5 nb for ^{200}W and from 23.5 nb for ^{203}Os to 1.8 nb for ^{206}Os. The stripping reactions are also investigated for the isotopic distribution of radon (Rn) and francium (Fr) production in the MNT reaction of $^{136}Xe + ^{208}Pb$. The four and five stripping protons enable the monitoring of the neutron shell evolution of $N = 126$. The available data of radon isotope production are nicely reproduced via the secondary decay spectrum (blue lines) by including the cluster transfer and dynamical deformation in the DNS model. A narrower isotopic distribution of francium production cannot be reproduced by the model, i.e., 15.9 μb for ^{220}Rn and 29.7 μb for ^{220}Fr in the calculations, but the lower cross section of 5.7 ± 1.1 μb for ^{216}Fr in experiments.

The closed neutron shell of $N = 126$ and the proton shell of $Z = 82$ are favorable for MNT fragment formation. The nuclear spectroscopies of shell evolution, in particular, for the nuclide properties beyond the β-stability line, are of importance for exploring nucleosynthesis in the r-process, i.e., the heavy element creation in binary neutron star merging. In the terrestrial laboratories, the neutron-rich heavy isotopes might be created via the MNT reactions. The shell effect enhances the fission barrier and enlarges the separation energy of the MNT fragments, which are favorable for the primary products and for the survival of the cold fragments via the binary fission and β decay. The isotonic and isotopic distributions of the MNT products formed in the reactions of $^{58,64,72}Ni + ^{198}Pt$ near the Coulomb barrier energies are shown in Fig. 3. It is obvious that the system $^{72}Ni + ^{198}Pt$ ($V_C = 212.2$ MeV) is available for the neutron-rich isotope production, e.g., the maximal cross section with 0.23 mb for ^{208}Pb and 2.6 nb for ^{202}Os. The reaction of $^{58}Ni + ^{198}Pt$ ($V_C = 228.2$ MeV) is favorable for the proton-rich isotope, e.g., 13.1 nb for ^{196}Pb and 0.12 nb for ^{193}Pb. The incident energy dependence of $^{64}Ni + ^{198}Pt$ ($V_C = 220.3$ MeV) is obvious for the proton-rich isotope production.

The beam energy influences the dissipation energy into the DNS and consequently the MNT fragment formation. The more local excitation energy is obtained with increasing the incident energy and leads to the wider isotopic distribution [60]. A number of rare isotopes might be created with more energetic nuclear collisions. However, decreased survival of the primary fragment is obtained by transfer dynamics. The competition of the diffusion of nucleon transfer and the survival of formed fragments leads to the isotopic structure of the final MNT fragments, which is associated with the beam energy and the colliding system. It is found that the total mass and charge distributions of the secondary fragments near the shell closure with $N = 126$ weakly depend on the bombarding energy in the MNT reaction of $^{136}Xe + ^{198}Pt$ [61]. Systematic investigation of the energy dependence on the fragment formation in the MNT reactions would be helpful for selecting the optimal beam energy in experiments. Shown in Fig. 4 are the isotopic distributions of platinum, iridium, osmium, and rhenium in the pick-up reactions of $^{64}Ni + ^{198}Pt$ and $^{72}Ni + ^{198}Pt$ at center-of-mass energies of 210, 220, and 230 MeV, respectively. Overall, the neutron-rich radioactive nuclide ^{72}Ni-induced reactions are favorable for the neutron-rich isotope production, in particular, at incident energies of 220 and 230 MeV, above the Coulomb barrier ($V_C = 212.2$ MeV). The maximal yields of the isotopic distributions deviate from the β-stability line to the neutron-rich region, i.e., 27.8, 1.58, 3.03, and 0.82 mb for ^{198}Pt, ^{197}Ir, ^{194}Os, and ^{191}Re, respectively.

In summary, the DNS model is improved by implementing the cluster transfer into the master equations, i.e., deuterons, tritons, ^{3}He, and α particles, in which the nucleon transfer and cluster effect are coupled to the temporal evolution of quadrupole deformation and dissipation of the relative motion energy and the angular momentum. The inclusion of cluster transfer in the DNS model is favorable for MNT fragment formation and leads to a broad isotopic distribution, and the distribution probability is associated with the cluster separation energy of the DNS fragment. The production cross sections of the MNT fragments transferring more than 20 nucleons are nicely consistent with the Argonne data. The neutron-rich isotopes of elements W and Os near $N = 126$ are predicted with cross sections above 10 nb in the MNT reactions of $^{136}Xe + ^{208}Pb$ at $E_{c.m.} = 450$ MeV. The system $^{72}Ni + ^{198}Pt$ is favorable for the production of neutron-rich nuclides of isotones with $N = 126$ and of isotopes with $Z = 82$. The production cross sections of isotones and proton-rich isotopes are associated with the beam energy. However, the neutron-rich nuclides are nearly independent of the beam energy.

This work was supported by the National Natural Science Foundation of China (Projects No. 12175072 and No. 12311540139) and the Talent Program of South China University of Technology (Project No. 20210115).

[1] D. Kennedy, Science **309**, 19 (2005).
[2] Yu. Ts. Oganessian, A. G. Demin, A. S. Iljinov, S. P. Tretyakova, A. A. Pleve, Yu. E. Penionzhkevich, M. P. Ivanov, and Yu. P. Tretyakov, Nucl. Phys. A **239**, 157 (1975).
[3] S. Hofmann and G. Münzenberg, Rev. Mod. Phys. **72**, 733 (2000).
[4] K. Morita, K. Morimoto, D. Kaji *et al.*, J. Phys. Soc. Jpn. **73**, 2593 (2004).

[5] G. Münzenberg, Nucl. Phys. A **944**, 5 (2015).
[6] Yu. Ts. Oganessian, A. V. Yeremin, A. G. Popeko *et al.*, Nature (London) **400**, 242 (1999); Yu. Ts. Oganessian, V. K. Utyonkov, Yu. V. Lobanov *et al.*, Phys. Rev. C **62**, 041604(R) (2000).
[7] Yu. Ts. Oganessian, V. K. Utyonkov, Yu. V. Lobanov *et al.*, Phys. Rev. C **74**, 044602 (2006).
[8] Yu. Ts. Oganessian and V. K. Utyonkov, Nucl. Phys. A **944**, 62 (2015).
[9] W. D. Myers and W. J. Swiatecki, Nucl. Phys. **81**, 1 (1966).
[10] A. Sobiczewski, F. A. Gareev, and B. N. Kalinkin, Phys. Lett. **22**, 500 (1966).
[11] M. Thoennessen, *The Discovery of Isotopes: A Complete Compilation* (Springer, Heidelberg, 2016).
[12] H. Sakurai, Front. Phys. **13**, 132111 (2018).
[13] S. Gales, AIP Conf. Proc. **1224**, 424 (2010).
[14] J. Wei *et al.*, Int. J. Mod. Phys. E **28**, 1930003 (2019).
[15] X. Chen, J. C. Yang, J. W. Xia *et al.*, Nucl. Instrum. Methods Phys. Res., Sect. A **920**, 37 (2019).
[16] A. G. Artukh, V. V. Avdeichikov, G. F. Gridnev, V. L. Mikheev, V. V. Volkov, and J. Wilczynski, Nucl. Phys. A **176**, 284 (1971).
[17] A. G. Artukh, G. F. Gridnev, V. L. Mikheev, V. V. Volkov, and J. Wilczynski, Nucl. Phys. A **211**, 299 (1973).
[18] A. G. Artukh, G. F. Gridnev, V. L. Mikheev, V. V. Volkov, and J. Wilczynski, Nucl. Phys. A **215**, 91 (1973).
[19] K. D. Hildenbrand, H. Freiesleben, F. Pühlhofer, W. F. W. Schneider, R. Bock, D. v. Harrach, and H. J. Specht, Phys. Rev. Lett. **39**, 1065 (1977).
[20] P. Glässel, D. v. Harrach, Y. Civelekoglu, R. Männer, H. J. Specht, J. B. Wilhelmy, H. Freiesleben, and K. D. Hildenbrand, Phys. Rev. Lett. **43**, 1483 (1979).
[21] K. J. Moody, D. Lee, R. B. Welch, K. E. Gregorich, G. T. Seaborg, R. W. Lougheed, and E. K. Hulet, Phys. Rev. C **33**, 1315 (1986).
[22] R. B. Welch, K. J. Moody, K. E. Gregorich, D. Lee, and G. T. Seaborg, Phys. Rev. C **35**, 204 (1987).
[23] H. M. Devaraja, S. Heinz, O. Beliuskina *et al.*, Phys. Lett. B **748**, 199 (2015).
[24] E. M. Kozulin, E. Vardaci, G. N. Knyazheva, A. A. Bogachev, S. N. Dmitriev, I. M. Itkis, M. G. Itkis, A. G. Knyazev, T. A. Loktev, K. V. Novikov, E. A. Razinkov, O. V. Rudakov, S. V. Smirnov, W. Trzaska, and V. I. Zagrebaev, Phys. Rev. C **86**, 044611 (2012).
[25] J. S. Barrett, W. Loveland, R. Yanez, S. Zhu, A. D. Ayangeakaa, M. P. Carpenter, J. P. Greene, R. V. F. Janssens, T. Lauritsen, E. A. McCutchan, A. A. Sonzogni, C. J. Chiara, J. L. Harker, and W. B. Walters, Phys. Rev. C **91**, 064615 (2015).
[26] Y. X. Watanabe *et al.*, Phys. Rev. Lett. **115**, 172503 (2015).
[27] V. V. Desai, W. Loveland, K. McCaleb, R. Yanez, G. Lane, S. S. Hota, M. W. Reed, H. Watanabe, S. Zhu, K. Auranen, A. D. Ayangeakaa, M. P. Carpenter, J. P. Greene, F. G. Kondev, D. Seweryniak, R. V. F. Janssens, and P. A. Copp, Phys. Rev. C **99**, 044604 (2019).
[28] E. M. Kozulin, V. I. Zagrebaev, G. N. Knyazheva *et al.*, Phys. Rev. C **96**, 064621 (2017).
[29] S. Wuenschel, K. Hagel, M. Barbui *et al.*, Phys. Rev. C **97**, 064602 (2018).
[30] T. Niwase *et al.*, Phys. Rev. Lett. **130**, 132502 (2023).
[31] T. Kurtukian-Nieto *et al.*, Phys. Rev. C **89**, 024616 (2014).
[32] Z. Q. Feng, G. M. Jin, and J. Q. Li, Phys. Rev. C **80**, 057601 (2009).
[33] G. G. Adamian, N. V. Antonenko, V. V. Sargsyan, and W. Scheid, Phys. Rev. C **81**, 024604 (2010).
[34] G. G. Adamian, N. V. Antonenko, V. V. Sargsyan, and W. Scheid, Phys. Rev. C **81**, 057602 (2010).
[35] A. Winther, Nucl. Phys. A **572**, 191 (1994).
[36] A. Winther, Nucl. Phys. A **594**, 203 (1995).
[37] V. I. Zagrebaev and W. Greiner, Nucl. Phys. A **944**, 257 (2015).
[38] A. V. Karpov and V. V. Saiko, Phys. Rev. C **96**, 024618 (2017).
[39] V. V. Saiko and A. V. Karpov, Phys. Rev. C **99**, 014613 (2019).
[40] C. Golabek and C. Simenel, Phys. Rev. Lett. **103**, 042701 (2009).
[41] K. Sekizawa and K. Yabana, Phys. Rev. C **88**, 014614 (2013).
[42] X. Jiang and N. Wang, Chin. Phys. C **42**, 104105 (2018).
[43] Z. Wu and L. Guo, Phys. Rev. C **100**, 014612 (2019).
[44] K. Sekizawa and S. Ayik, Phys. Rev. C **102**, 014620 (2020).
[45] J. Tian, X. Wu, K. Zhao, Y. Zhang, and Z. Li, Phys. Rev. C **77**, 064603 (2008).
[46] K. Zhao, Z. Li, X. Wu, and Y. Zhang, Phys. Rev. C **88**, 044605 (2013).
[47] K. Zhao, Z. Li, N. Wang, Y. Zhang, Q. Li, Y. Wang, and X. Wu, Phys. Rev. C **92**, 024613 (2015).
[48] Z. Q. Feng, G. M. Jin, J. Q. Li, and W. Scheid, Phys. Rev. C **76**, 044606 (2007); Nucl. Phys. A **816**, 33 (2009).
[49] W. Nörenberg, Z. Phys. A **274**, 241 (1975).
[50] S. Ayik, B. Schürmann, and W. Nörenberg, Z. Phys. A **277**, 299 (1976).
[51] Z. Q. Feng, G. M. Jin, F. Fu, and J. Q. Li, Nucl. Phys. A **771**, 50 (2006).
[52] R. Mattiello, H. Sorge, H. Stöcker, and W. Greiner, Phys. Rev. C **55**, 1443 (1997).
[53] Z. Q. Feng, Phys. Rev. C **102**, 044604 (2020).
[54] G. Wolschin and W. Nörenberg, Z. Phys. A **284**, 209 (1978).
[55] H. M. Devaraja, S. Heinz, D. Ackermann, T. Göbel, F. P. Heßberger, S. Hofmann, J. Maurer, G. Münzenberg, A. G. Popeko, and A. V. Yeremin, Eur. Phys. J. A **56**, 224 (2020).
[56] P. H. Chen, F. Niu, Y. F. Guo *et al.*, Nucl. Sci. Tech. **29**, 185 (2018).
[57] C. Peng and Z. Q. Feng, Eur. Phys. J. A **58**, 162 (2022).
[58] V. Zagrebaev and W. Greiner, Phys. Rev. Lett. **101**, 122701 (2008).
[59] F. G. Kondev, M. Wang, W. J. Huang, S. Naimi, and G. Audi, Chin. Phys. C **45**, 030001 (2021).
[60] F. Niu, P.-H. Chen, Y.-F. Guo, C.-W. Ma, and Z.-Q. Feng, Phys. Rev. C **96**, 064622 (2017).
[61] Z. Q. Feng, Phys. Rev. C **95**, 024615 (2017).